Sensing and Bio-Sensing Research 7 (2016) 153–161

Contents lists available at ScienceDirect

Sensing and Bio-Sensing Research

journal homepage: www.elsevier.com/locate/sbsr

Nanopore formation on Au coated pyramid under electron beam irradiations (plasmonic nanopore on pyramid)

Seong Soo Choi [a,*], Myoung Jin Park [a], Tokutaro Yamaguchi [a], Chul Hee Han [a], Sae-Joong Oh [a], Sung In Kim [b], Jung Ho Yoo [b], Kyoung Jin Park [b], Yong-Sang Kim [c], Nam Kyou Park [d]

[a] Research Center for Nano-Bio Science, SunMoon University, Ahsan, Chungnam 31460, South Korea
[b] National Nanofabrication Center, Daejeon, South Korea
[c] School of Electronics and Electrical Engineering, Sung Kyunkwan University, South Korea
[d] School of Electrical Engineering, Seoul National University, South Korea

ARTICLE INFO

Article history:
Received 30 August 2015
Received in revised form 16 January 2016
Accepted 18 January 2016

Keywords:
Electron beam irradiation
Surface diffusion
Carbon contamination
Au cluster
Ostwald ripening

ABSTRACT

There have been tremendous interests about the single molecule analysis using a sold-state nanopore. The solid-state nanopore can be fabricated either by drilling technique, or diffusion technique by using electron beam irradiations. The solid-state SiN nanopore device with electrical detection technique recently fabricated, however, the solid-state Au nanopore with optical detection technique can be better utilized as the next generation single molecule sensor. In this report, the nanometer size openings with its size less than 10 nm on the diffused membrane on the 200 nm Au pyramid were fabricated by using field emission scanning electron microscopy (FESEM) electron beam irradiations, transmission electron microscopy (TEM), etc. After the sample was being kept under a room environment for several months, several Au (111) clusters with ~6 nm diameter formed via Ostwald ripening are observed using a high resolution TEM imaging. The nanopore with Au nanoclusters on the diffused membrane can be utilized as an optical nanopore device.

1. Introduction

There have been many studies related to fabrication of the solid state nanopores using various techniques such as ion sculpting, high energy electrons beams due to the possible ultrafast genome sensing capabilities of the nanopore [1,2]. So far, the solid-state SiN, SiO_2 nanopore for an electrical detection technique has been successfully fabricated using electron beam irradiation techniques such as field emission scanning microscopy (FESEM) and transmission electron microscopy (TEM) [3–6]. However, the plasmonic Au nanopores have yet to be fabricated and can be utilized as optical detection bio sensing devices [7,8]. A nanopore can be fabricated by either drilling a membrane, or shrinking a nano-aperture size down to a diameter of ~10 nm or less, by using an electron beam irradiation technique. When electron beam irradiates on the specimen using TEM, depending upon the ratio of membrane thickness to the aperture diameter, the nanometer size hole will either shrink or become open [1]. This phenomenon is attributed to the surface tension on the membrane, which become viscous from electron beam irradiations. Resizing of hole on the viscous membrane or on the heated metallic membrane is well documented [9,10]. Under electron beam irradiation using FESEM, the hole always shrinks, regardless of the ratio of membrane thickness to hole diameter [3–5]. For accelerating energy less than 5 keV of FESEM, the penetration depth of electron will be less than 50 nm, therefore, most of electron energy will be deposited in the ~10^2 nm thick specimen [11]. Temperature rise on the specimen irradiated by electron beam with an energy less than 20 keV is reported previously by Casting et al. [12,13]. Local temperature rise dependent upon the electron beam probe diameter, electron beam current, and voltage, and thermal conductivity of the bulk specimen can be higher than the Au melting temperature (1337 K). Considering the fact that vapor pressure of the Au-C system was reported to be ~3×10^{-5} Torr at Au melting temperature [14], local temperature rise in the specimen can be high enough to make the specimen viscous and vaporized in the high vacuum environment (~10^{-7} Torr or lower).

For electron energy range of ~10^2 keV of TEM, most of energy will be transmitted and local temperature rise would depend on inelastic collisions; Coulomb explosion, thermal spikes. [15,16]. Shrinking and opening of the nanometer size hole on the membrane are reported [1,5]. Drilling of nanopore on the metallic foil under focused electron beam irradiation is also reported, and it can be attributed to electron beam induced thermal spikes [17–20]. Local temperature rise from thermal spikes can be as high as the vaporization temperature, and it can also present transient melting and rapid motion of Au particles [21–23]. Charging effects from insufficient contacts with specimen

* Corresponding author.
E-mail address: sscphy2010@gmail.com (S.S. Choi).

http://dx.doi.org/10.1016/j.sbsr.2016.01.009

supports and the size of the particle also present melting temperature change [15,21 and 23].

The hydrocarbon contamination has been a problem for fabrication of the metallic nanopore [24,25]. When electron beam currents irradiate over the micrometer size area, the annular contamination will be formed with higher carbon contamination buildup at the periphery of the irradiated area than at the center. This stems from the surface diffusion of the absorbed hydrocarbon on the specimen toward the center of the irradiation area. The diffused hydrocarbons will be cross-linked to the surface when electron beam irradiates on the surface. Hence carbon contamination ring will be formed and it will be difficult for carbon atoms to diffuse into the center of the irradiating area [26,27].

In addition, low nuclear mass of hydrogen results in a threshold energy for displacement energy below 2 keV. The C-H bond energy is 4.36 eV and its corresponding displacement energy is very low [26]. Hence, during electron beam irradiations, hydrogen atoms will be knocked out by electron bombardments, and the mobile surface hydrocarbon deposits are converted into amorphous carbons. The resulting amorphous carbon adsorbates are cross-linked to the surface and become stable under further electron irradiations.

Carbon encapsulation of Au atoms under heating and Au evaporation during TEM imaging are recently reported by others [28,29]. It is reported that Au clusters smaller than 1 nm in diameter cannot be resolved due to low contrast on the amorphous substrate by TEM, and that Au cluster formation and island formation on the amorphous films is observed after 4 months of aging under room temperature environments. This phenomenon is attributed to Ostwald ripening process; large particles are thermodynamically more favorable than small particles [30,31]. Hence, small particles has tendency to condense on the larger particles. Therefore, all the small particles will shrink and larger particles will grow, and the size of larger particles will increase. When gold atoms are covered by carbons, the Au atoms become more stable with carbon atoms than without carbons [30]. In this report, nanopore formation, shrinking and opening of the electron beam induced membrane, and the Au cluster formation process will be investigated.

2. Experimental process

2.1. Microfabrication of Au apertures on the pyramid

The pyramidal nanometer size apertures on top of the oxide pyramid array were fabricated using conventional Si microfabrication techniques. The (20 × 20) micrometer patterns were engraved using such as photolithography followed by tetramethylammonium hydroxide (TMAH) alkaline wet etching, stress-induced thermal oxidation at 950 °C, and metal sputter deposition. The stress-induced thermal oxidation provided the thinner oxide at the apex of the pyramid. During backside Si etching of more than 10 h using TMAH, the thin oxide at the apex will be etched away and the circular oxide aperture is formed at the apex [31–34]. The two step metal sputter deposition was carried out by using a DC 400 watt electron beam sputter. The detailed fabrication process is given as in Fig. 1.

Fig. 2 presents the fabricated SiO_2 pyramidal array in (a) and an oxide aperture with a ~260 nm diameter (b). A 200 nm thick Au film was sputter-deposited by using a DC 400 W power electron beam sputter for 120 s under 40 sccm Ar flow vacuum condition. Fig. 1(c) and (d) presents the FESEM image and the TEM image of the same Au nano-aperture. The nanoflower-type Au aperture size is shown in (c). The TEM image in (d) shows an Au nanosize hole with (31 nm × 46 nm) size, surrounded by a gray Au membrane, by using 200 keV TEM (JEM- 2010).

2.2. Nano-opening formation under electron beam irradiations

The various electron beam irradiations were carried out in order to reduce the aperture diameter down to a ~10^0 nm nanometer, the

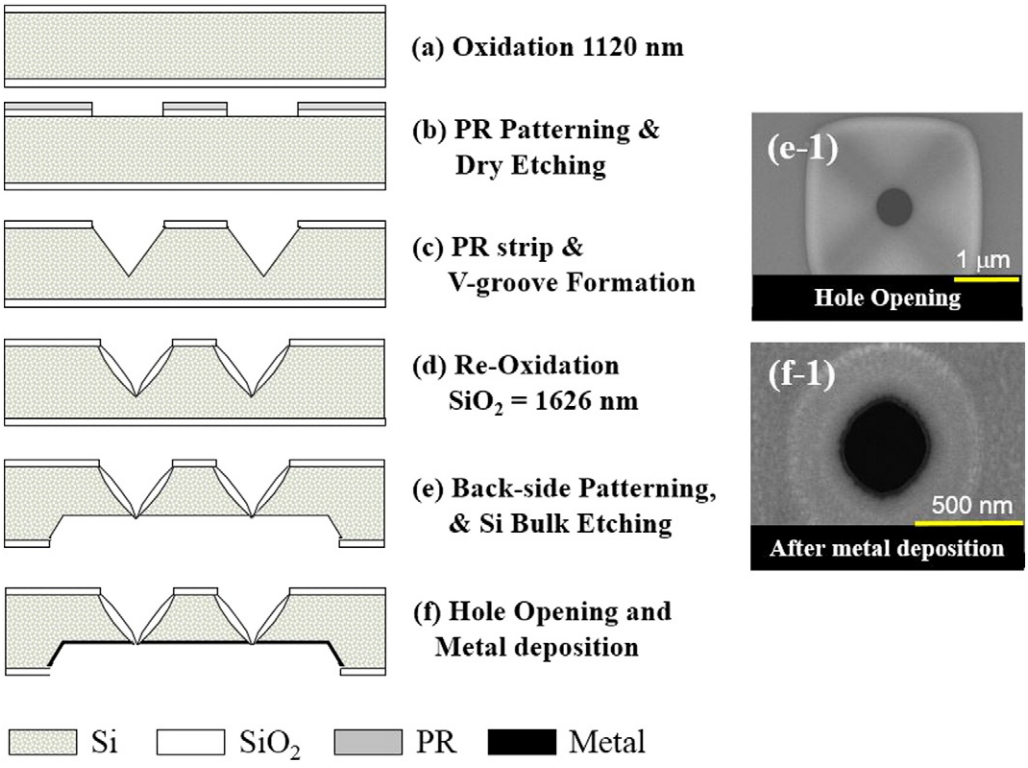

Fig. 1. Schematic drawing for microfabrication process. Thermal oxidation in (a) followed by PR patterning and dry etching (b), V-groove formation (c), reoxidation (d), and backside Si bulk etching (e) were followed. After nano-aperture opening (e), a 200 nm Au film was sputter-deposited by using DC 400 W electron beam sputter (f), and FESEM images for an oxide aperture on pyramid and an Au nanoflower-type aperture are shown in (e-1) and (f-1), respectively.

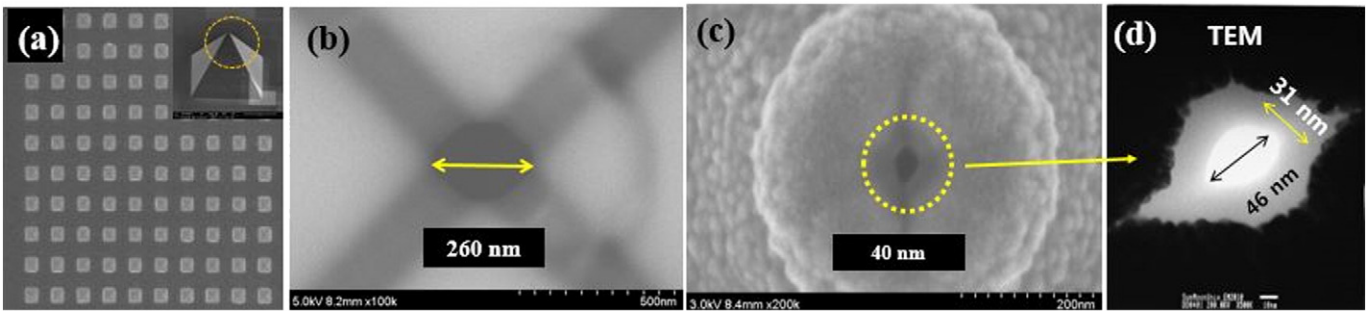

Fig. 2. FESEM images show the top view of the oxide pyramid array and the tilted view of a pyramid in (a), and an oxide aperture with ~260 nm on the apex of the pyramid in (b). The 40 nm long SEM image of nano-aperture on the Au nanoflower is shown inside the dotted circle in (c). A TEM image for the same nano-aperture is shown in (d). The (31 nm × 46 nm) size nano-opening area surrounded by a gray membrane area inside the dark Au film is shown.

electron beam irradiation techniques such as TEM (JEM-2010 and JEM-3011HR,), FESEM (JSM 6400), and electron probe microscopy (EPMA, JSA-8100). TEM can provide high electron voltages ranging from 100 keV to 300 kV and the currents with ~ order of 100 pA. EPMA can provide the adjustable probe diameter and currents with electron voltage range of (1 ~ 30) kV. During low energy electron beam irradiation with low energy electron beam irradiation on the bulk samples, the temperature rise, ΔT can be given as below:

$$\Delta T = 4.8E_0 i/k\,d \quad (1)$$

where E_0 is the primary electron energy, i is the absorbed beam current, k is the thermal conductivity of the substrate, and d is the electron beam probe diameter [12,13]. The recent FESEM has a beam probe diameter with ~10^0 nm. The probe current is order of ~nA. The thermal conductivity of the bulk Au is ~3.18 W/cm K. For 20 keV primary electron beam energy using EPMA. The temperature rise for electron beam exposure using EPMA will be above the bulk Au melting temperature (1337 K) for a 2 μm probe diameter and a 100 s exposure time. With a proper exposure time, the temperature would be high enough to melt an Au thin film. Considering the bulk melting point of Au, 1337 K in atmospheric pressure and the vapor pressure of Au at 1337 K is ~3×10^{-5} Torr, the evaporation process and the surface tension from the Au viscous liquid state will become important for 10^{-8} Torr of an electron beam annealing condition, such as FESEM and TEM. Furthermore, the melting temperature for Au nanoparticle depends on the size of the Au particle [23].

First, we drilled slit type holes and circular holes on the apex of the 200 nm Au deposited SiO_2 pyramid using a dual beam FIB (FEI, Helios NanoLab). Then, numerous electron beam irradiations at 2 keV on the FIB drilled apertures were carried out to resize the drilled apertures using FESEM, followed by TEM imaging. Fig. 3(a) presents a nanoslit with (3.65 nm × 119.8 nm) size. Under electron beam irradiations using TEM (JEM-3011HR) at 300 keV and 511 pA, the width of a nanoslit was widened to 10.12 nm from 3.65 nm and the length of the slit (119.8 nm) was reduced to ~45 nm in (b). For 6 min of 532 pA electron beam irradiations at 300 keV, the TEM image reveals a 10.60 nm width of the slit and no shape change of the slit in (c).

FIB drilled circular-type apertures with diameters less than 100 nm, i.e., 96.5 nm and 73.9 nm were drilled as in Fig. 4(a) and (c), respectively. The Au cluster islands formed during the FIB drilling are shown. Under 5 min, 1.4 nA FESEM electron beam irradiations at 2 keV to obtain fast shrinking, the nanosize openings of 3.79 nm and 5.57 nm on the diffused membranes were formed as in (b) and (d), respectively. In these particular samples series, it was quite difficult to control the size of the diffused membranes using FESEM electron beam irradiation. Due to low penetration depth of less than 10 nm at 2 keV, the deposited energy density becomes very high enough to make local temperature rise above the melting points [13]. This would result in the fast surface diffusion and fast shrinking of the diffused membrane.

2.3. Controlling the aperture openings using TEM electron beam irradiations

Electron beam irradiations at 300 keV, 511 pA TEM electron beams were carried out to resize the openings on the FESEM diffused membranes. Openings of (20 nm × 57 nm) on the diffused membrane in Fig. 5(a) were widened to (28 nm × 58 nm) after a 10 min irradiation in Fig. 5(b). Opening of (16 nm × 30 nm) in Fig. 5(c) was also widened to (27 nm × 39 nm) after 12 min irradiation in Fig. 5(d). Slow opening of a nanometer size hole is clearly shown under a 512 pA electron beam irradiation at 300 keV in the video file [Supplementary materials file name: Opening under 512 pA].

In order to resize the aperture, electron beam irradiations on the samples with beam currents ranging from 511 pA down to 250 pA, and 100 pA were performed. However, no shape shrinking was observed for these beam currents. We only observed disappearance of the thin membrane formed during FIB drilling. Fig. 6 presents TEM images of a 86 nm wide Au aperture after 200 nm Au deposition followed by 30 keV FIB drilling. The uneven elliptical aperture was initially formed during ~15 h long backside Si etching to reveal the oxide

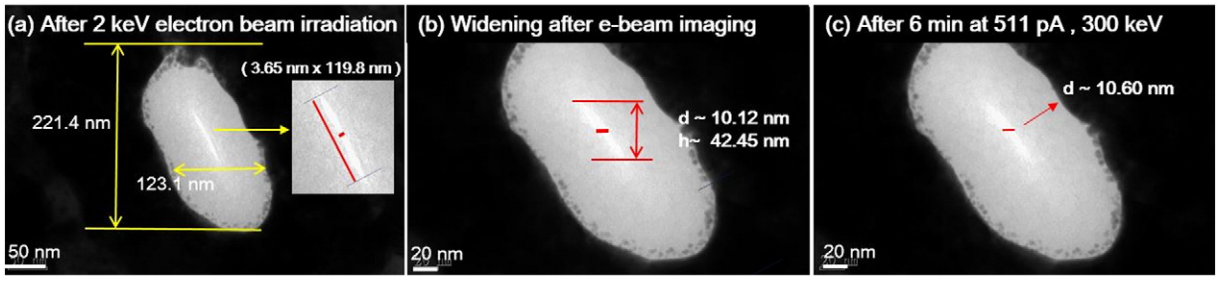

Fig. 3. TEM images of a (3.65 nm × 119.8 nm) slit-type opening after 2 keV electron beam irradiation (a), of slightly enlarged opening with d ~ 10.12 nm and h ~ 42.45 nm during 300 keV TEM imaging in (b), and after 6 min of electron beam irradiation at 300 keV, no shape change, i.e., only 0.48 nm width opening was observed in (c).

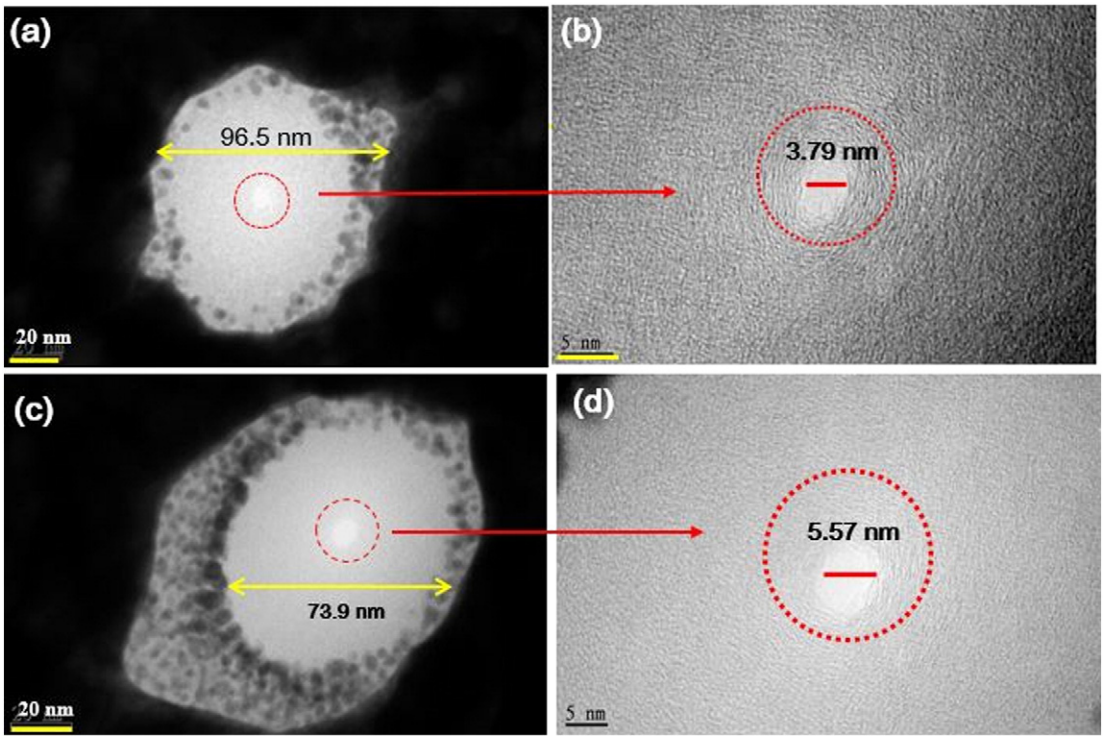

Fig. 4. Openings of 3.79 nm diameter and 5.57 nm diameter on the diffused membranes are presented in (a) and (b), (c) and (d), respectively. Electron beam irradiations at 2 keV, 1.4 nA FESEM were performed after FIB drilling on top of the pyramids. (Sample ID TEM 3-20-1).

pyramid, a 200 nm Au film was sputtered deposited followed by FIB drilling. After FIB drilling, a circular-type hole with an 86 nm width is shown in Fig. 6(a). Under an electron beam irradiation at 300 keV for 50 min, rather than shrinking, we observed disappearance of the membrane formed during FIB drilling. Widening of the hole from 86 nm to 98 nm was observed in Fig. 6(b). The Au nanosize clusters formed during FIB drilling process are also shown at the periphery of the drilled Au aperture. Under a 1.5 keV FESEM electron beam irradiation for 10 min, an opening of a 45 nm width on the diffused membrane is presented in Fig. 6(c). The increased numbers of Au clusters at the periphery of the diffused membrane with a roughened surface are also presented. (See Fig. 7.)

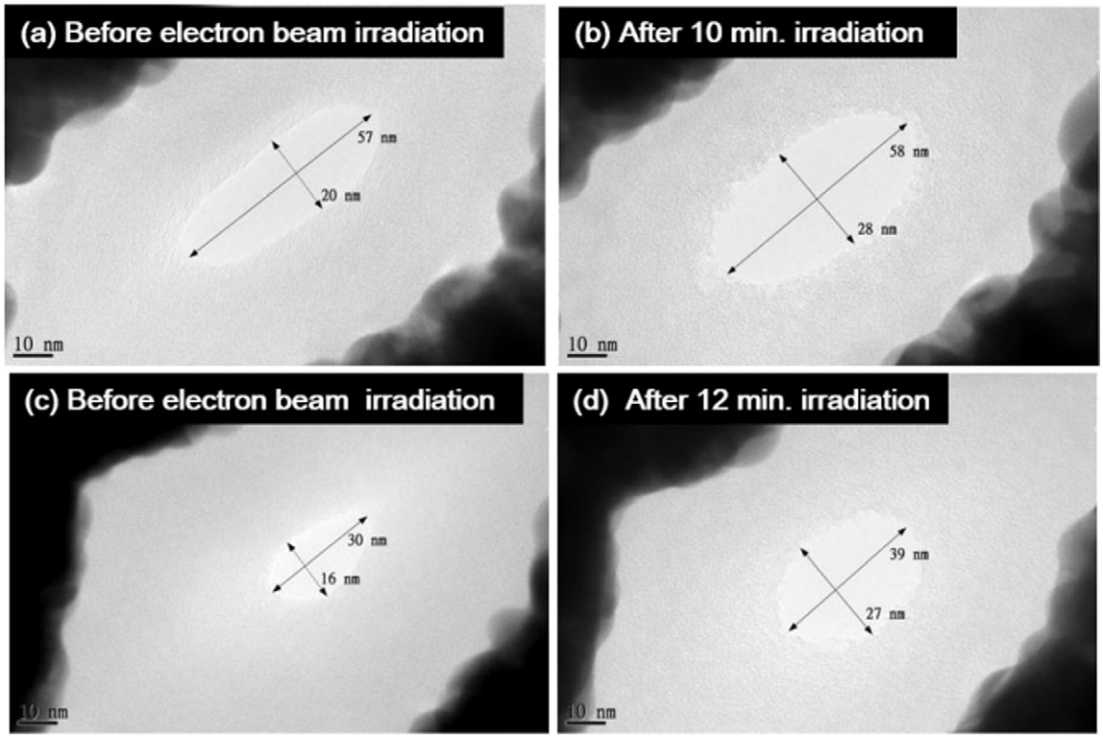

Fig. 5. The TEM images of two openings with (20 nm × 57 nm) and with (16 nm × 30 nm) on the diffused membranes before 511 pA electron beam irradiations are shown in (a) and (c), respectively. After 511 pA electron beam irradiations at 300 keV, the reduced openings with (28 nm × 58 nm) and with (27 nm × 39 nm) are presented in (b) and (d), respectively.

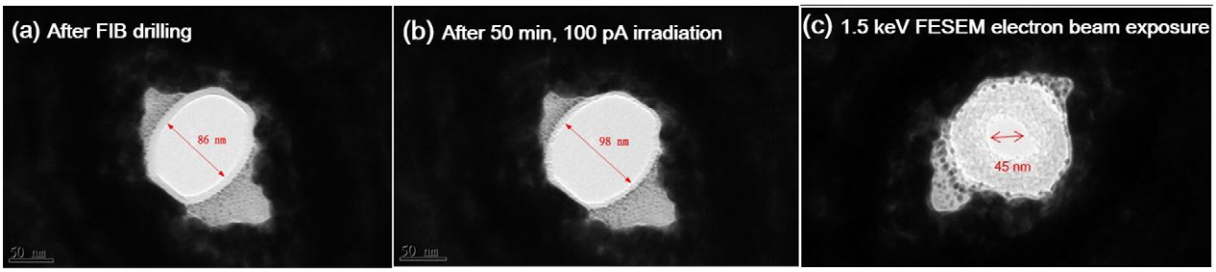

Fig. 6. TEM images of the Au nano-apertures are presented after FIB drilling (a), after 100 pA, 300 keV TEM electron beam irradiation for 50 min (b), after 1.5 keV FESEM electron beam irradiation for 10 min (c).

For Au apertures with its diameter larger than 50 nm, we found that resizing was very difficult and only to make the thin membrane formed during FIB drilling disappear, either by evaporation or migration as shown in Fig.8. For electron beam irradiations with 100 pA beam currents, the widening of the diffused membrane is presented in Fig. 8. We drilled an Au aperture with its diameter less than 50 nm on top of pyramid. Fig. 8 presents the TEM images of a FIB-drilled aperture with successive electron beam irradiations with 51 pA. A FIB drilled egg-shape aperture with a 34 nm width is shown in Fig. 8(a). The thin membrane with a ~10 nm width around the periphery of the aperture formed during FIB drilling is also shown. Under a 51 pA electron beam irradiation for 45 min., the size of the aperture becomes reduced and the width is measured to be 21 nm in Fig. 8(b). Then, after 11 days later under the room environment, the sample was reinserted into the TEM chamber. The shape change of the aperture is presented and the width of the aperture is measured to be ~12 nm in Fig. 8(c). This phenomenon can be attributed to the atomic diffusion on the membrane. For another 43 min electron beam irradiation at 51 pA, the resized aperture of (2.4 nm × 17 nm) is shown in Fig. 8(d). This nonuniform resizing can be due to uneven atomic density distribution around the egg-shape aperture. Each electron beam density profiles at the detector for the apertures of (b), (c) and (d) are also presented in (b-1), (c-1) and (d-1), respectively. The video file for "Au aperture reduction" is presented [Supplementary materials file name: Au aperture reduction]. In this video file, the Au atomic diffusion is clearly seen under electron beam irradiations.

In addition, we also carried out resizing experiments dependent upon the electron beam current density using EPMA. EPMA can provide the adjustable probe diameter and beam diameter. Fig. 9 presents the widening and the shrinking phenomena of the slit-type aperture depending upon the electron beam current density. The (368.3 nm long × 130.3 nm wide) of the long slit-type hole was drilled on top of the pyramidal structure by using focused ion beam techniques (Dual-Beam Helio NanoLab) in Fig. 9(a). Then, a 5 keV electron beam irradiation was carried out for 5 min by using FESEM to reduce the size of the drilled hole down to (113.8 nm × 15.0 nm) in (b), a slight widening of the nanopore size to (119.4 nm × 45.4 nm) was shown in (c), under a 100 s irradiation with 20 keV, 40 nA/μm^2, and 4 μm probe diameter by using EPMA. However, a shrinking of the hole down to (67.3 nm × 14.7 nm) size is shown under a 200 s exposure with a 1 nA/μm^2, and a 4 μm EPMA probe diameter in (c). Finally, shrinking down to (11.7 nm × 5.9 nm) size was shown after another electron beam irradiation with 1 nA/μm^2 for 100 s. During these processes, after electron beam irradiation by using EPMA, the sample was taken out from the EPMA chamber and was inserted into the TEM chamber for TEM imaging at 200 keV.

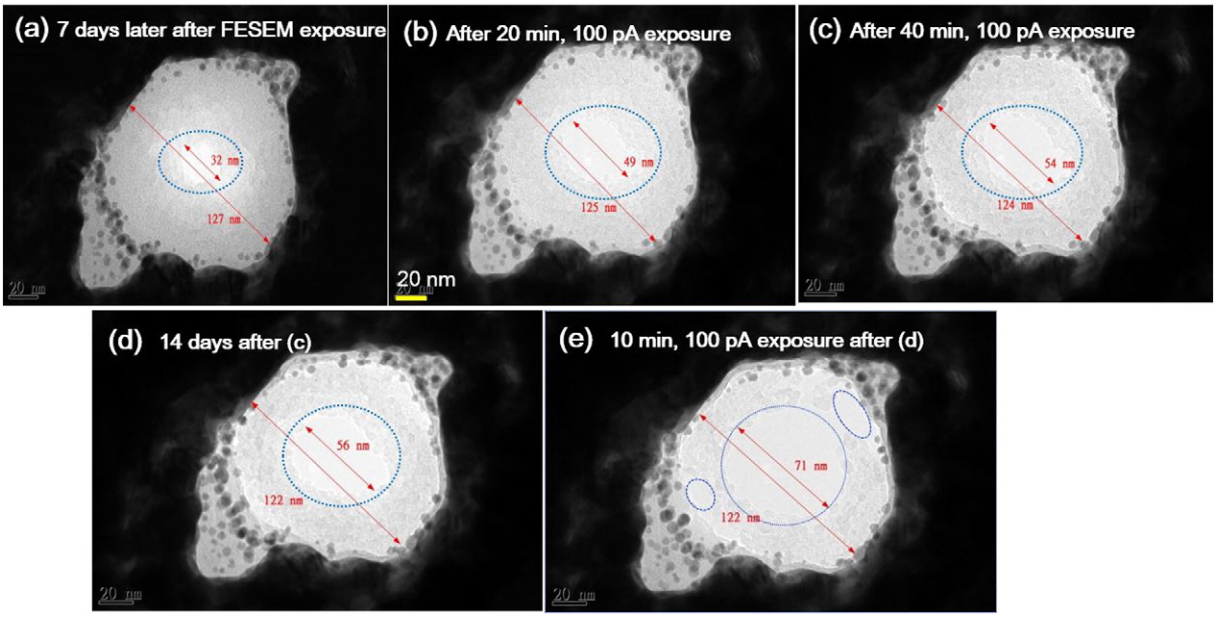

Fig. 7. The TEM images of a FIB drilled Au aperture on pyramid after successive electron beam irradiations focused on the imaged areas with 100 pA are shown. Widening of a nano-hole on the diffused membrane by FESEM electron irradiations from 32 nm diameter to 49 nm is shown after 300 keV, 100 pA TEM electron beam irradiation for 20 min (b). After 14 days in air, the membrane temperature cooled down and the hole-opening becomes widened to 56 nm. After another 10 min. Electron beam irradiation with 100 pA, the open void area was widened to 71 nm due to electron beam damage. In addition, two open void areas near the Au islands are also shown. [Blue dotted circled areas in (e)].

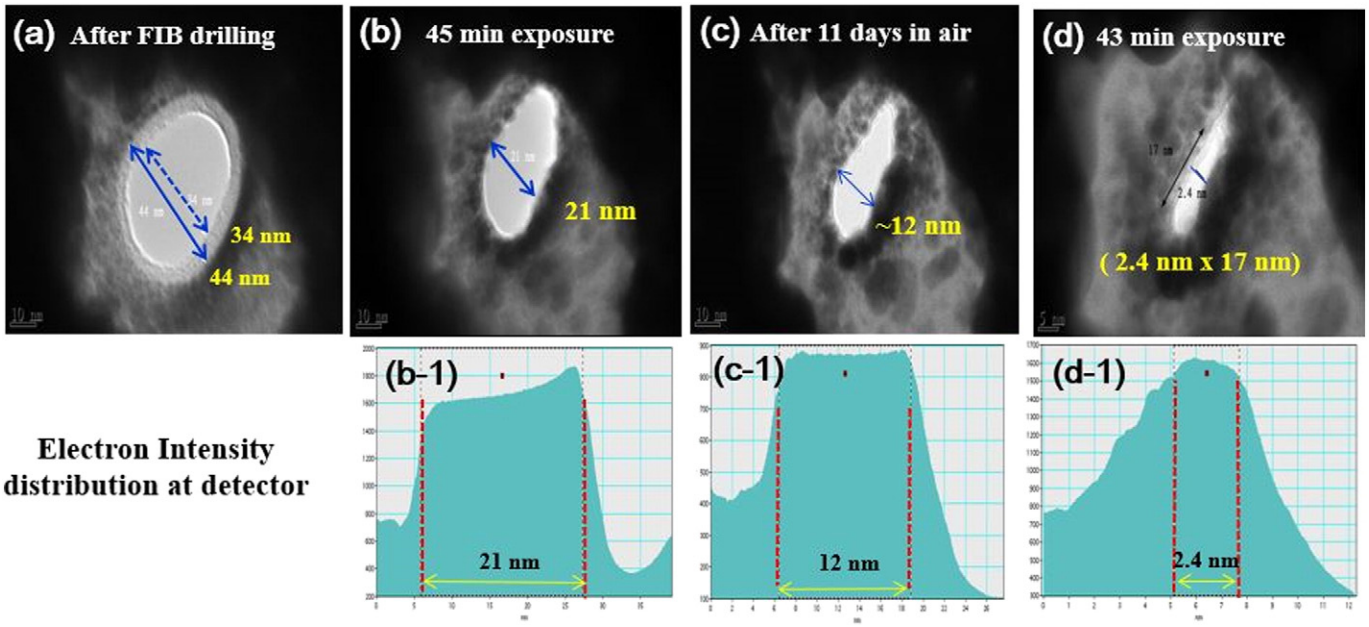

Fig. 8. TEM images of FIB drilled Au aperture on pyramid followed by successive 51 pA electron beam irradiations. An aperture with a 34 nm width is shown along with a diffused thin membrane with ~10 nm width formed during FIB drilling. After 45 min 51 pA electron beam irradiations at 300 keV, the size of the aperture opening is reduced to be ~ (21 nm × 55 nm). After 11 days under room environment, the diffused membrane became shrunk and the width of the opening area is shown to be 12 nm in (c). After another 43 min electron beam irradiation, the size of the opening hole is measured to be (2.4 nm × 17 nm) in (d). The electron density profiles at the detector of the (b), (c) and (d) are presented in (b-1), (c-1), and (d-1), respectively.

2.4. Energy dispersive X-ray analysis

2.4.1. Au atomic diffusion during FESEM electron beam irradiation

We carried out a resizing experiment to confirm Au atomic diffusion during FESEM electron beam irradiation. The 2 keV FESEM electron beam irradiation for 10 min was utilized to resize the aperture with a 942.5 nm diameter and a 5 keV EDAX analysis was carried out. After 10 min electron beam irradiation, the diameter of the circular aperture is reduced to 757.5 nm. The difference is 113.8 nm as in Fig. 10. Then, the energy dispersive X-ray analysis was carried out by using 5 keV electron beam to better activate the X-rays from Au atoms. Fig. 11 presents the EDAX data from the point (X2) on the 200 nm bulk Au area and the point (X1) on the diffused area. The carbon concentrations in the diffused region is measured to be higher than in the 200 nm Au bulk region as in Table 1. The ratios of Au atoms to C atoms in the diffused area and in the 200 nm Au bulk area are 0.266 and 0.486, respectively. This data confirms Au presence into the diffused region. The video file for Au atomic diffusion under electron beam irradiation on an Au aperture with a 500 nm diameter is presented [Supplementary file name: 500 nm Hole FESEM 2 keV 0.69 nA].

2.4.2. Elemental analysis on the diffused membrane using 200 keV STEM focused probe of a 1.5 nm probe diameter

The chemical analysis for the electron beam induced membrane was also performed using EDAX system with STEM (JEOL 2100F). The EDAX analysis using 200 keV STEM can provide a better qualitative results than EDAX analysis using FESEM due to a larger and better detector system at 200 keV STEM. The focused electron beam probe with a 1.5 nm diameter is set to 2.5 nA probe current at 200 keV and the duration time is ~40 s. Three different samples irradiated by FESEM electron beam are prepared for EDAX analysis in Fig. 12. Table 2 presents the ratios of Au atoms to C atoms on the different spots on each sample. Three different points are selected; a center point on the diffused area, a peripheral point on the diffused area, a third point on the 200 nm Au bulk area. The gold atomic percents at the center area for sample (a), (b), and (d) is 15.31%, 2.82%, and 2.31%, respectively. The ratio of gold atomic percent to carbon atomic percent for the diffused gray areas for sample (a), (b), and (c) is ~0.12, 0.09, and 0.09, respectively. However, the ratios of gold atomic percent to carbon atomic percent on the 200 nm Au bulk area for (a), (b), (c), and (d) are 2.24, 2.48, 2.15, and 3.26, respectively. During EDAX point analysis on the center

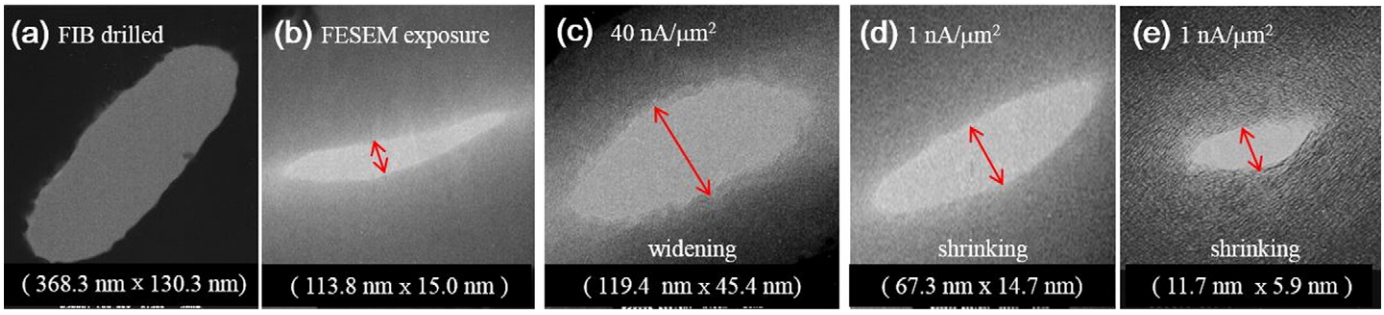

Fig. 9. TEM image of FIB drilled Au slit-type aperture is shown in (a). Widening and shrinking of the opened hole on the diffused membrane are presented depending upon the electron beam current density using EPMA. After FESEM exposure at 20 keV, the pore size of (113.8 nm × 15.0 nm) on the diffused membrane is reduced to (113.8 nm × 15 nm) in (b). Then, after 100 s electron exposure with 40 nA/μm^2 electron beam current density, the nanopore is widened to (119.4 nm × 45.4 nm) in (c). However, for an electron beam exposure with the beam current density of 1 nA/μm^2, the pore was shrunk to (67.3 nm × 14.7 nm) in (d). After another electron beam exposure at 1 nA/μm^2, the pore was shrunk again to (11.7 nm × 5.9 nm) in (e).

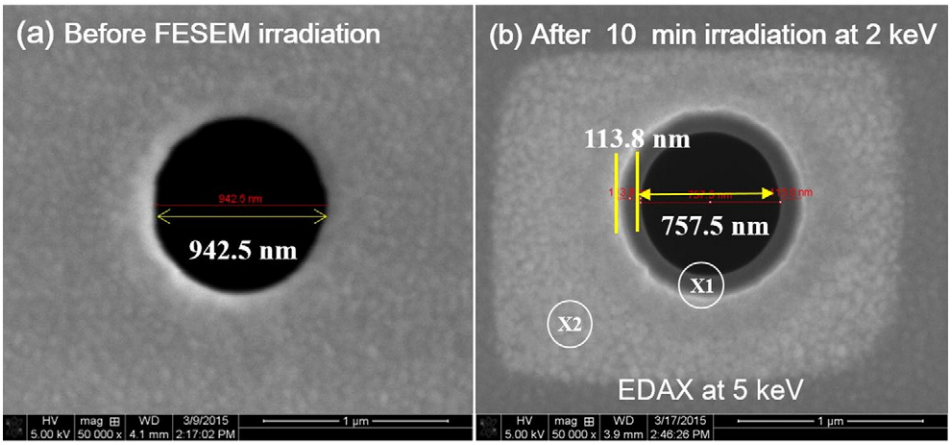

Fig. 10. FESEM images of FIB drilled Au nano-aperture before in (a), and after 2 keV FESEM electron beam irradiations in (b). Energy dispersive X-ray analysis at 5 keV was performed for elemental analysis on the diffused membrane.

in the sample (b), the center region is damaged and the open void with 30.4 nm diameter is presented as inserted in Fig. 12(c). This can be due to "electron beam induced drilling" from 2.5 nA probe currents with a 1.5 nm probe diameter. The beam shifting due to an unstable electron beam irradiation can be attributed to a wide void open area of 30.4 nm. However, we are not able to observe same "opening effect" from the sample (a) and sample (d). These data reveal the followings; (i) the diffused membrane contains both gold atoms and carbon atoms. (ii) At the center, the ratio of the Au atom concentration to the carbon atom concentration is highest; the richest Au atom concentration at the center, (iii) carbon contamination ring: The higher carbon concentration in the diffused region close to the 200 nm Au film region than any other points is observed.

2.5. Observation of Au cluster formation on the diffused membrane

Fig. 13 shows TEM images of a diffused membrane inside a 200 nm thick Au film after various electron beam irradiations. Several high energy electron beam irradiations using 200 keV TEM were performed on the diffused membrane. Fig. 13(a) shows a TEM image after electron beam irradiations for drilling a nanometer size hole by using 2.5 nA, 200 keV electron beam with a 1.5 nm probe diameter. There are no particles or clusters on the diffused membrane. However, after the sample was kept in a desiccator for one year under a room environment, we observed a surface morphology change and several Au clusters on the diffused membrane in (b). The shape of the large opening was changed and the small void opening was completely closed (b). The formation of the Au clusters can be attributed to Ostwald ripening effect; the larger particles would become larger and larger from the expense of smaller particles in order to minimize the system surface energy. The Au atoms below the TEM detection limit on the diffused are not able to detect or to obtain the TEM imaging [28]. The Au (1×1) surface on the a-C membrane does exhibit more stable than the Au (1×1) surface without carbon membrane [30]. Therefore, Au atoms diffuse together with carbon atoms under electron beam irradiations, and Au particles coalesce together via Ostwald ripening on the a-C membrane, then form the Au clusters under a room environment [29–31]. The cluster with an Au (111) lattice spacing with 2.3 nm for 10 atomic rows is shown in (c). The influence on the Au cluster formation on the electron beam irradiation is still under investigation.

3. Results and Discussion

The nanopores on the 200 nm Au deposited pyramids were fabricated using various electron beam irradiation techniques such as TEM, FESEM, and EPMA. Initially, the SiO_2 pyramids were fabricated by using Si mcirofabrication techniques, followed by an electron beam sputter deposition of a 200 nm thick Au film. FIB milling was carried out on the deposited Au nano-apertures in order to obtain the apertures with a diameter of ~100 nm or less. In order to obtain the nanometer size opening on the FIB-milled apertures in a controllable manner, the high energy electron beam irradiations were utilized.

(i) Fabrication of a nanometer size slit with (3.65 nm × 119.8 nm) size and a circular openings with ~6 nm diameter or less on the pyramid; we performed electron beam irradiations with 2 keV

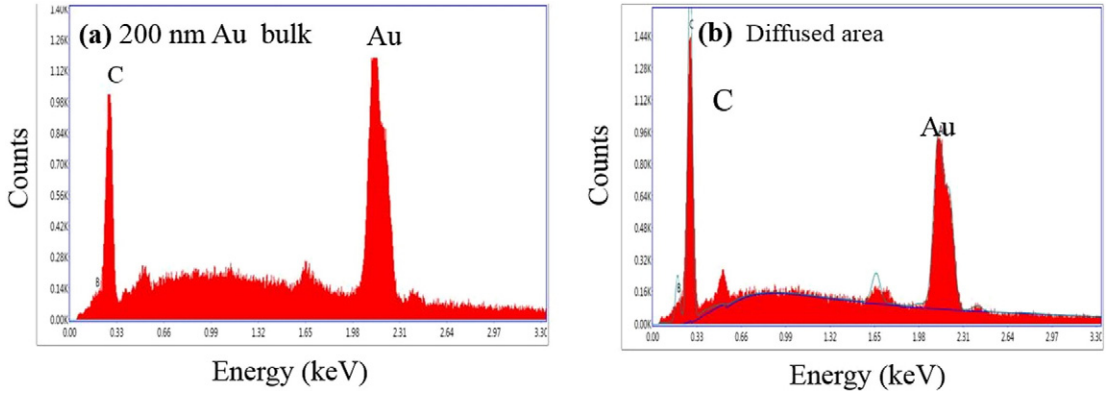

Fig. 11. EDAX data for carbon and gold on the 200 nm thick Au area (a) and on the diffused area (b). The higher concentration of carbon on the point (X1) than at point (X2) on the 200 nm thick Au bulk area is shown. Au concentration in the diffused area is shown under a 2 keV 1.4 nA electron beam irradiation in (b).

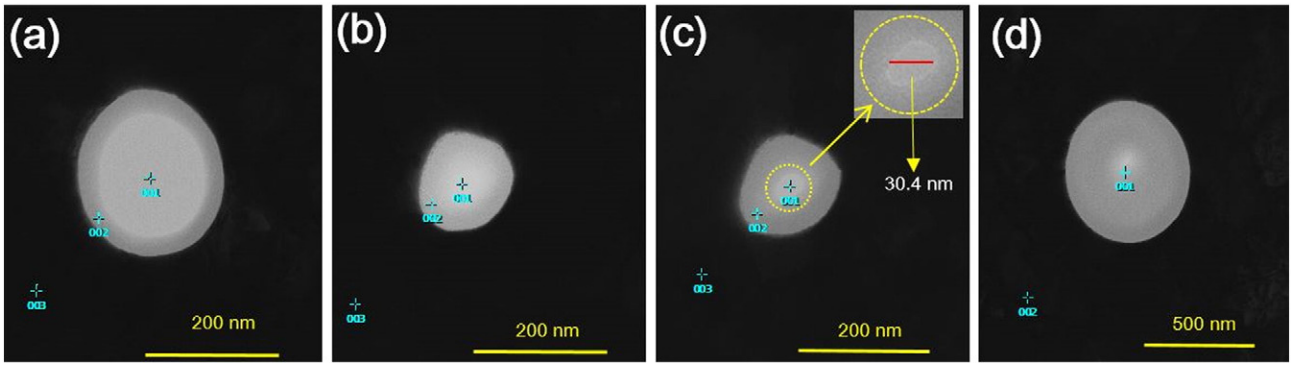

Fig. 12. TEM images of the diffused membranes on the three samples for EDAX point analysis. Three different points from 3 samples are chosen for EDAX analysis. The image (c) is taken after 200 keV EDAX analysis on the sample (b). The center area was damaged and the open void area with 30.4 nm width is shown in (c) (inserted on top right).

FESEM on the slit-type aperture and on the circular aperture on the apex of the pyramids to obtain a nanometer size opening on the FESEM electron beam induced membrane.

(ii) Forming a void opening on the diffused Au-C membrane under a high energy electron beam irradiation at 300 keV using TEM; Dependency upon the electron beam currents ranging from 511 pA down to 100 pA to control "opening of the hole" on the diffused membrane by the FESEM electron beam irradiation were examined. "Opening phenomena of the nanometer size holes" were observed under electron beam irradiations with beam current ranging from 511 pA to 100 pA on the FESEM diffused membranes. "Opening," or "closing" of the nanometer size hole on the diffused membrane can be attributed to either vaporization of the atoms, or diffusion in the diffused membrane. The evaporation can be induced either by electron beam induced heat, or by knock-on displacement at 300 keV electron beam irradiations, considering the facts that the threshold energy for Au nanoparticle sputtering is as low as 1.9 eV.

(iii) "Shrinking phenomena" under of the FIB drilled Au aperture; Shrinking of the aperture width from 44 nm down to 21 nm was observed, under a 45 min electron beam irradiation with 51 pA at 300 keV. The Au aperture of (21 nm wide × 55 nm long) was shrunken to 12 nm width after the sample was kept in a desiccator for one week. Under another electron irradiation for 43 min, the Au aperture was resized to a (2.4 nm wide × 17 nm long) aperture. Due to nonuniform surroundings of the aperture, the original egg-shape aperture is shrunken to a narrow slit-type long aperture.

(iv) Resizing of nanometer size opening on the diffused membrane were observed depending upon electron beam currents density; A long slit type aperture with (368.3 nm × 130.3 nm) size was irradiated initially with 20 keV SEM to reduce the aperture down to (112.8 nm × 15 nm) aperture. Then, the aperture was widened to a (119.4 nm × 45.3 nm) aperture for electron beam current density of 40 nA/μm^2. Under the successive electron beam irradiations with 1 nA/μm^2 electron beam current density at 20 keV, the aperture was shrunken to (67.3 nm × 14.7 nm) and (11.7 nm × 5.9 nm), respectively.

(v) Au presence in the diffused membrane and a carbon contamination ring: A 5 keV FESEM EDAX analysis after 2 keV electron beam irradiation reveals that the diffused membrane reveals Au particle and amorphous carbon. Another EDAX analysis using scanning TEM at 200 keV also presents the followings; The annular contamination ring is observed with more carbon contamination buildup at the periphery of the diffused area than at the center, (a) highest atomic concentration of Au at the center of the diffused membrane, (b) the highest C concentration at the periphery of the diffused membrane (carbon contamination ring).

(vi) Au cluster and Au island formation via Ostwald ripening under the room environments. Several Au clusters with ~6 nm width are observed after being kept in a desiccator under room environments for one year. The Au atoms below the TEM detection limit on the diffused area are not able to detect or to obtain the TEM imaging. The formation of Au clusters can be attributed to Au atom migration at room temperature and coarsening from Ostwald ripening effect.

We investigated formation of a nanometer size hole of ~10^0 nm inside an Au aperture under various electron beam irradiations. Depending upon temperature rise of the specimen, the surface would either evaporate, or migrate. For FESEM electron beam irradiations, all of the

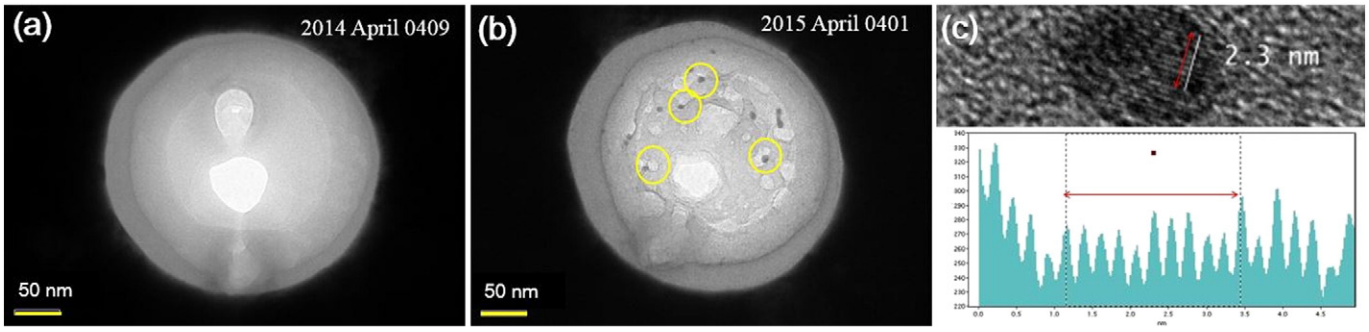

Fig. 13. TEM images of a diffused membrane after various electron beam irradiations. A large opening and a small void opening area in the diffused membrane from various electron beam irradiations are shown in a large and a small blue dotted circle in (a). No particles or clusters are shown in (a). However, after one year later, the Au clusters with ~6 nm width are shown in yellow dotted circles (b). The shape of the opening was also changed (b). The lattice spacing of the Au cluster is measured to be 2.3 nm for 10 lattice rows in (c). The transmitted electron beam profile through the Au cluster through the cluster at the detector is shown (bottom). This spacing matches with Au (111) lattice spacing.

Table. 1
Data for atomic percents of the Au and C on the diffused membrane and the 200 nm thick Au film are presented. The lower ratio of (Au/C) is shown on the diffused membrane than on the 200 nm thick Au film.

	Atomic %		
	Carbon C(K)	Gold Au(M)	Au/C
Diffused membrane	58.53	15.82	0.266
200 nm Au film	47.5	23.1	0.486

Table. 2
Ratio of gold to carbon on the selected area of the samples.

	Ratio (Au/C)			
		Center	Gray membrane	200 nm thick Au (black area)
Sample a (circle)	Atomic %	15.31	0.12	2.24
	Mass %	249	2.01	37.51
Sample b (closed small circle)	Atomic %	2.82	0.09	2.48
	Mass %	46.08	1.46	40.72
Sample c (after EDAX, pore damaged and opened)	Atomic %	N/A	0.09	2.15
	Mass %	N/A	1.43	35.25
Sample d	Atomic %	2.31	N/A	3.26
	Mass %	38.13	N/A	54.38

incident electron energy will be deposited, and the local temperature rise is high enough to create solid-phase diffusion of atoms resulted in "shrinking" phenomenon. For TEM electron beam irradiations, most of electron energy will be transmitted and inelastic scattering such as Coulomb explosion and thermal spike would be contributed to local temperature rise. Under high electron beam irradiations with high beam intensities ranging from 511 pA to 100 pA at 300 keV, the opening of the irradiated diffused membrane area become "widened," due to vaporization of the atoms. Under a 50 min irradiation with 100 pA, 300 keV on the egg-shaped 86 nm wide Au aperture, the 200 nm thick Au aperture did not show any shape change. However, we observed an Au aperture shrinking and Au migration under a 51 pA electron beam irradiation for 45 min. The resized Au aperture was slowly shrunken down to 21 nm. This "shrinking" process can be attributed to Au atom migration from the viscous Au film under irradiation. This process was rather slow compared with other shrinking process under FESEM electron beam irradiations. We observed several Au clusters and islands formed on the electron beam induced membrane by using High resolution TEM. The Au atoms in the diffused carbon membrane below TEM detection limit coalesced together and forms the Au clusters via Ostwald ripening.

4. Conclusion

We successfully fabricated the nano-openings on the Au-C diffused membrane inside the Au aperture on the pyramidal apex. The nanopore on the 200 nm thick Au pyramidal structure can be an excellent candidate for next generation single molecule bio sensor. The Au aperture and Au cluster formed on the Au-C diffused membrane can provide the enhancement of surface enhanced Raman optical signal up to 10^6 fold increase. The enhanced optical intensity from Au aperture can be utilized as optically driven technique for single molecule, while the enhanced optical intensity from Au cluster on the diffused membrane can be utilized as an optical detection technique for single molecule. Therefore, a nano-opening with controlled proper size can be utilized as the next generation single molecule sensor.

Supplementary data to this article can be found online at http://dx.doi.org/10.1016/j.sbsr.2016.01.009.

Acknowdgments

This work was supported by the research funding program (Nanopatterned optical nanopore for single molecule analysis and manipulation, 2015R1D1A1A09056781056781) under the Basic Science Research Program through the National Research Foundation (NRF) funded by the Ministry of Education, Science and Technology and the Global Research Laboratory funding (GRL; Nanoplasmonic Integrated Circuits for Ultrafast Information Processing, KRF Grant No. K20815000003, 2008-00580).

References

[1] A.J. Storm, J.H. Chen, X.S. Ling, H.W. Zanbergen, C. Dekker, Nat. Mater. 2 (2003) 537–540.
[2] J. Li, Stein, C. McMullan, D. Branton, M.J. Aziz, J.A. Golovchenko, Nature 412 (2001) 166–169.
[3] A.S. Prabhu, K.J. Freedman, J.W.F. Robertson, Z. Nikolov, J.J. Kasianowicz, M.J. Kim, Nanotechnology 22 (2011) 425302.
[4] H. Chang, S.M. Iqbal, E.A. Stach, A.H. King, N.J. Zaluzec, R. Bashir, Appl. Phys. Lett. 88 (2006) 103109.
[5] C.J. Lo, T. Aref, A. Bezryadin, Nanotechnology 17 (2006) 3264–3267.
[6] S.S. Choi, M.J. Park, T. Yamaguchi, S.I. Kim, K.J. Park, N.K. Park, Appl. Surf. Sci. 310 (2014) 196–203.
[7] F. Eftekharl, C. Escobedo, J. Ferreira, X. Duan, E.M. Girotto, A.G. Broto, R. Gordon, D. Sinton, Anal. Chem. 81 (2009) 4308–4311.
[8] M.P. Jonsson, A.B. Dahlin, L. Feuz, S. Petronis, F. Hook, Anal. Chem. 82 (2010) 2087–2094.
[9] G.I. Taylor, D.H. Michael, J. Fluid Mech. 58 (1973) 625–639.
[10] M. Lanxner, C.L. Bauer, R. Scholz, Thin Solid Films 150 (1987) 323–335.
[11] K. Kanaya, S. Okayama, J. Phys. D. Appl. Phys. 5 (1972) 43–58.
[12] R. Castaing, Application of electron probes to local chemical and crystallographic analysisPh.D. thesis University of Paris, Jun. 8 1951.
[13] T.W. Basil, M.P. Menguc, R.R. Balance, J. Heat, Transfer 126 (2004) 566–576.
[14] E.H. Copland, Long Term Measurements of the Vapor Pressure of Gold in the Au-C System, NASA/CR 2009-215498, 2009.
[15] A. Howie, Nature 320 (1986) 684.
[16] E.M. Bringa, R.E. Johnson, Phys. Rev. Lett. 88 (2002) 165501.
[17] T. Yokota, M. Murayama, J.M. Howe, Phys. Rev. Lett. 91 (2003) 265504.
[18] J.-G. Lee, H. Mori, Sci. Technol. Adv. Mater. 5 (2004) 51–55.
[19] T.J. Bullough, Philos. Mag. A 75 (1997) 69–85.
[20] S. Bysakh, M. Shimojoa, K. Mitsuishi, K. Furuya, J. Vac. Sci. Technol. B 22 (2004) 2620–2627.
[21] N. Doraiswamy, L.D. Marks, Surf. Sci. 348 (1996) L67–L69.
[22] P. Williams, Appl. Phys. Lett. 50 (1987) 1760.
[23] Ph. Buffat, J.-P. Borel, Phys. Rev. A 13 (1976) 2287.
[24] J.J. Hren, Chapter 10, Barriers to AEM: contamination and etching, Introduction to Analytical Electron Microscopy, Plenum Press, New York 1979, pp. 481–505.
[25] R.F. Egerton, P. Li, M. Malac, Micron 35 (2004) 399–409.
[26] R.F. Egerton, Microsc. Res. Tech. 75 (2012) 1550–1556.
[27] Ludwig Reimer, Chapter 10. Specimen damage by electron irradiation, Physics of Image formation, Transmission Electron Microscopy, Springer series in Optical Science, fifth ed.Springer 2008, pp. 447–450.
[28] R. Werner, M. Wanner, G. Schneider, D. Gerthsen, Phys. Rev. B 72 (2005) 045426.
[29] B. Westenfelder, J.C. Meyer, J. Biskupek, S. Kurasch, F. Scholz, C.E. Krill III, U. Kaiser, Nano Lett. (2011) 5123–5127.
[30] L.D. Marks, Phys. Rev. Lett. 51 (1983) 1000–1002.
[31] K. Yoshida, A. Bright, N. Tanaka, J. Electron Microsc. 61 (2012) 99–103.
[32] S.S. Choi, J.T. Ok, D.W. Kim, M.Y. Jung, M.J. Park, J. Kor. Phys. Soc. 45 (2004) 1659–1663.
[33] D.W. Kim, M.J. Park, C.H. Han, S.S. Choi, Nanotechnology 16 (2005) S304–S307.
[34] S.S. Choi, M.Y. Jung, M.S. Song, M.J. Park, D.W. Kim, Proc. SPIE 5736 (2005) 105–109.